LETTERS

Nanomechanical measurements of a superconducting qubit

M. D. LaHaye[1], J. Suh[1], P. M. Echternach[3], K. C. Schwab[2] & M. L. Roukes[1]

The observation of the quantum states of motion of a macroscopic mechanical structure remains an open challenge in quantum-state preparation and measurement. One approach that has received extensive theoretical attention[1–13] is the integration of superconducting qubits as control and detection elements in nanoelectromechanical systems (NEMS). Here we report measurements of a NEMS resonator coupled to a superconducting qubit, a Cooper-pair box. We demonstrate that the coupling results in a dispersive shift of the nanomechanical frequency that is the mechanical analogue of the 'single-atom index effect'[14] experienced by electromagnetic resonators in cavity quantum electrodynamics. The large magnitude of the dispersive interaction allows us to perform NEMS-based spectroscopy of the superconducting qubit, and enables observation of Landau–Zener interference effects—a demonstration of nanomechanical read-out of quantum interference.

Dispersive frequency shifts resulting from the non-resonant interaction of a single atom and a macroscopic photon cavity were first demonstrated over 20 years ago[15], and ultimately have enabled beautiful demonstrations of the quantum nature of light and investigations of quantum decoherence[14]. Some of the most impressive of such measurements include the non-destructive observation of individual microwave photons[16] and the preparation of 'Schrödinger-cat' states of a single cavity mode[17]. Similar effects in superconducting qubits have also been used to detect the Fock states of a coplanar waveguide resonator[18] and the dressed-states of a microwave-driven Cooper-pair box (CPB) qubit[19].

It has been appreciated for some time that a nanomechanical resonator coupled to a superconducting qubit should be formally identical to cavity quantum electrodynamics (CQED) systems, such as a simple harmonic oscillator coupled to a two-level quantum system[1–13]. Furthermore, because of the large frequency difference between typical superconducting qubits and NEMS, a coupling regime that is analogous to the dispersive limit of CQED should exist naturally and, in a similar manner, enable the preparation and measurement of highly non-classical nanomechanical entangled states[6,11–13] and Fock states[2,7–9,11]. In this work, as a first step in implementing these more advanced proposals, we realize dispersive coupling of a CPB qubit and a nanomechanical resonator, and demonstrate, through measurements of the nanoresonator's CPB-state-dependent frequency shift, that the interaction is consistent with the simple picture of a harmonic oscillator coupled to a two-level quantum system.

Our nanomechanical resonator is the fundamental in-plane flexural mode of a suspended silicon nitride nanostructure (Fig. 1a). Its fundamental-mode response can be well described as a damped simple harmonic oscillator with characteristic resonant frequency $\omega_{\mathrm{NR}}/2\pi = 58\,\mathrm{MHz}$ (Fig. 1c), effective mass $M \approx 4\times10^{-16}\,\mathrm{kg}$, spring constant $K = M\omega_{\mathrm{NR}}^2 \approx 60\,\mathrm{N\,m^{-1}}$ and damping rate $\kappa = \omega_{\mathrm{NR}}/Q$, where Q ranges between ~30,000 and ~60,000 (Fig. 1c), depending on the temperature and the resonator's coupling to the measurement circuit and the CPB. Similar to the case for an electromagnetic oscillator, a Hamiltonian operator for the nanoresonator can be written in terms of creation, $\hat{a}^\dagger$, and annihilation, $\hat{a}$, operators, yielding $\hat{H}_{\mathrm{NR}} = \hbar\omega_{\mathrm{NR}}(\hat{a}^\dagger\hat{a}+1/2)$, where $\hbar = h/2\pi$ is the reduced Planck constant and the quanta in the mode, of which there are $N = \langle\hat{a}^\dagger\hat{a}\rangle$, are now mechanical quanta.

A split-junction CPB qubit[20], formed from two Josephson tunnel junctions and a superconducting aluminium loop, is coupled to the nanoresonator through capacitance, C_{NR} (Fig. 1a). The CPB is well described by a simple spin-1/2 Hamiltonian[21], $\hat{H}_{\mathrm{CPB}} = (E_{\mathrm{el}}\hat{\sigma}_z - E_{\mathrm{J}}\hat{\sigma}_x)/2$, where $\hat{\sigma}_z$ and $\hat{\sigma}_x$ are Pauli matrices in the CPB's charge basis. The first term in $\hat{H}_{\mathrm{CPB}}$ is the electrostatic energy difference, $E_{\mathrm{el}} = 8E_{\mathrm{C}}(n_{\mathrm{CPB}} + n_{\mathrm{NR}} - n - 1/2)$, between the nth and $(n+1)$th charge states, with the charging energy, $E_{\mathrm{C}} = e^2/2C_\Sigma$, determined by the electron charge, e, and the CPB island's total capacitance, $C_\Sigma = C_{\mathrm{NR}} + C_{\mathrm{CPB}} + 2C_{\mathrm{J}}$, where C_{J} is the capacitance of each Josephson junction and C_{CPB} is the capacitance between the CPB island and a nearby gate electrode. Here $n_{\mathrm{CPB}} = C_{\mathrm{CPB}}V_{\mathrm{CPB}}/2e$ and $n_{\mathrm{NR}} = C_{\mathrm{NR}}V_{\mathrm{NR}}/2e$ are the polarization charges (in units of Cooper pairs) applied by the gate electrode and the nanoresonator, which are held at potentials V_{CPB} and V_{NR}, respectively (Fig. 1b). The second term in $\hat{H}_{\mathrm{CPB}}$ is the Josephson energy of the junctions, $E_{\mathrm{J}} = E_{\mathrm{J0}}|\cos(\pi\Phi/\Phi_{\mathrm{o}})|$, where Φ is the externally applied magnetic flux, $\Phi_{\mathrm{o}} = h/2e$ is the flux quantum and E_{J0} is the maximum Josephson energy. From the diagonalization of $\hat{H}_{\mathrm{CPB}}$ (ref. 21), we find the CPB ground, $|-\rangle$, and excited, $|+\rangle$, states to be separated by the transition energy $\Delta E = \sqrt{E_{\mathrm{el}}^2 + E_{\mathrm{J}}^2}$, where E_{C}/h and E_{J0}/h typically are ~10 GHz.

Displacement (by x) of the nanoresonator results in linear modulation of the capacitance between the nanoresonator and CPB, $C_{\mathrm{NR}}(x) \approx C_{\mathrm{NR}}(0) + (\partial C_{\mathrm{NR}}/\partial x)x$, which modulates the electrostatic energy of the CPB through n_{NR} and E_{C}, resulting in the interaction Hamiltonian[2] $\hat{H}_{\mathrm{int}} = \hbar\lambda(\hat{a}+\hat{a}^\dagger)\hat{\sigma}_z$, where

$$\lambda \approx \frac{4n_{\mathrm{NR}}E_{\mathrm{C}}}{\hbar}\frac{1}{C_{\mathrm{NR}}}\frac{\partial C_{\mathrm{NR}}}{\partial x}x_{zp} \qquad (1)$$

is the capacitive coupling constant and $x_{\mathrm{zp}} = \sqrt{\hbar/2M\omega_{\mathrm{NR}}}$. For the parameter values used in this work (Supplementary Information), equation (1) yields $|\lambda/2\pi| \approx 0.3$–$2.3\,\mathrm{MHz}$.

The formal connection to CQED becomes clear when the full system Hamiltonian, $\hat{H} = \hat{H}_{\mathrm{NR}} + \hat{H}_{\mathrm{CPB}} + \hat{H}_{\mathrm{int}}$, is transformed to the energy eigenbasis of the qubit:

$$\hat{H} = \hbar\omega_{\mathrm{NR}}\hat{a}^\dagger\hat{a} + \frac{\Delta E}{2}\,\hat{\sigma}_z + \hbar\lambda(\hat{a}+\hat{a}^\dagger)\left(\frac{E_{\mathrm{el}}}{\Delta E}\hat{\sigma}_z - \frac{E_{\mathrm{J}}}{\Delta E}\hat{\sigma}_x\right) \qquad (2)$$

(where $\hat{\sigma}_z$ and $\hat{\sigma}_x$ are now Pauli matrices in the CPB's energy basis). Equation (2) is similar to a Jaynes–Cummings-type Hamiltonian[14]. With the qubit and nanoresonator far-detuned (that is, for

[1]Kavli Nanoscience Institute, Condensed Matter Physics, MS 114-36, [2]Applied Physics, California Institute of Technology, Pasadena, California 91125, USA. [3]Jet Propulsion Laboratory, California Institute of Technology, Pasadena, California 91109, USA.

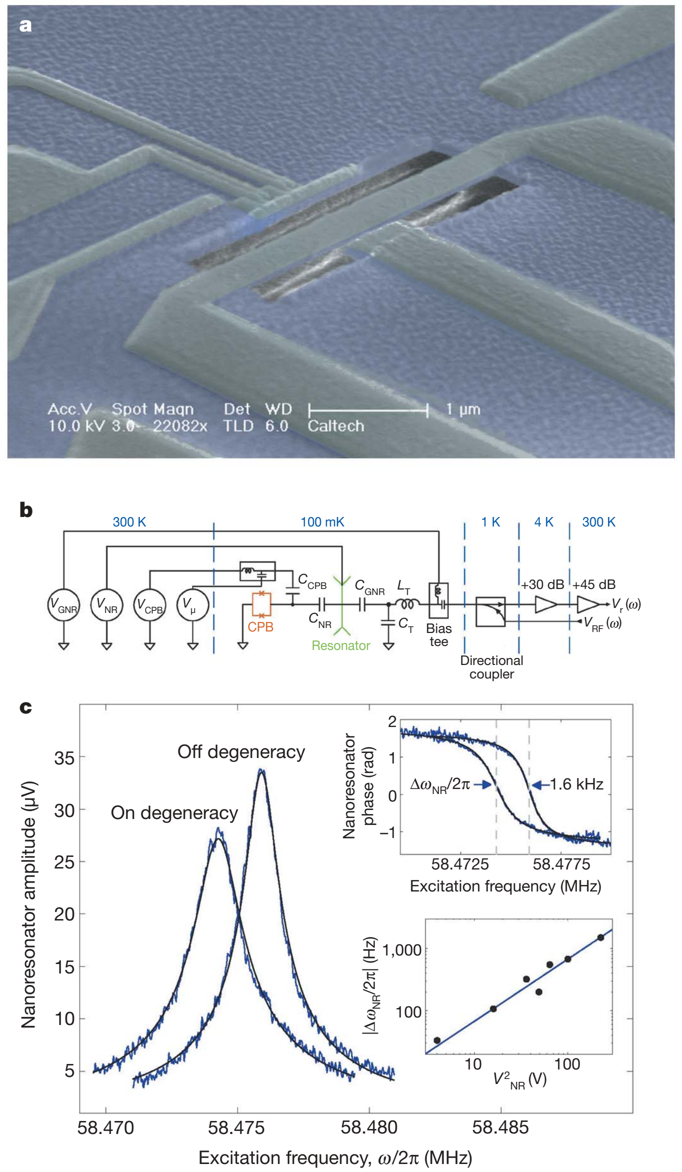

Figure 1 | Device and measurement circuit description, and driven frequency response of the nanoresonator. **a**, Colourized scanning electron micrograph of a device similar to the one measured. The nanoresonator is formed from low-stress silicon nitride with a thin coating (~80 nm) of aluminium for applying V_{NR}. The CPB is formed from aluminium during the same deposition steps as the nanoresonator. It is positioned at a distance ~300 nm from the nanoresonator, yielding the mutual capacitance $C_{\mathrm{NR}} = 43$ aF. Adjacent to the CPB is an aluminium electrode for applying V_{CPB}. Another aluminium electrode is situated ~100 nm from the opposite side of the nanoresonator, for actuating the nanoresonator and measuring $\Delta\omega_{\mathrm{NR}}/2\pi$. **b**, Circuit schematic for measuring $\Delta\omega_{\mathrm{NR}}/2\pi$ using radio-frequency reflectometry (Supplementary Information). For typical values of the d.c. voltages V_{NR} and V_{GNR}, where V_{GNR} is applied to the actuation electrode and used to tune the coupling of the nanoresonator to the measurement circuit, the excitation signal, $V_{\mathrm{RF}}(\omega)$, drives the nanoresonator at resonance ($\omega = \omega_{\mathrm{NR}}$) to 1–10-pm root-mean-squared amplitude or an effective occupation of ~10^3–10^5 quanta. The nanoresonator's response is transformed by L_{T} and C_{T} for matching to a cryogenic amplifier. After amplification at room temperature (~300 K), the signal, $V_{\mathrm{r}}(\omega)$, is fed to a radio-frequency lock-in for detection (Supplementary Information). **c**, The nanoresonator's amplitude (main panel) and phase (upper inset) versus excitation frequency, ω, for n_{CPB} biased on and off a charge degeneracy and $E_{\mathrm{J}}/h \approx 10$ GHz. The solid black lines each denote a fit to a harmonic oscillator response. Lower inset: magnitude of the nanoresonator frequency shift, $|\Delta\omega_{\mathrm{NR}}/2\pi|$ (black circles) as a function of V_{NR}^2 for $E_{\mathrm{J}}/h \approx 11$–12 GHz and V_{CPB} biased at a charge degeneracy. The solid blue line is a fit to $|\Delta\omega_{\mathrm{NR}}/2\pi| = AV_{\mathrm{NR}}^2$, where A is a proportionality constant.

$\hbar|\lambda|\sqrt{N} \ll |\Delta E - \hbar\omega_{\mathrm{NR}}|$), the dispersive coupling limit is realized, and, to lowest order, the system undergoes a shift in energy that can be viewed as a CPB-dressed correction to the nanoresonator's frequency[2]:

$$\frac{\Delta\omega_{\mathrm{NR}}}{2\pi} = \frac{\hbar\lambda^2}{\pi}\frac{E_{\mathrm{J}}^2}{\Delta E(\Delta E^2 - (\hbar\omega_{\mathrm{NR}})^2)}\langle\hat{\sigma}_z\rangle \qquad (3)$$

For $\Delta E > \hbar\omega_{\mathrm{NR}}$, $\Delta\omega_{\mathrm{NR}}/2\pi < 0$ when the CPB resides in the ground state ($\langle\hat{\sigma}_z\rangle = -1$) and $\Delta\omega_{\mathrm{NR}}/2\pi > 0$ when the CPB fully occupies the excited state ($\langle\hat{\sigma}_z\rangle = 1$). The dependence of $\Delta\omega_{\mathrm{NR}}/2\pi$ on $\langle\hat{\sigma}_z\rangle$ is in close analogy to the single-atom refractive shift[14] that arises in the dispersive limit of CQED. In our system, $\Delta E \gg \hbar\omega_{\mathrm{NR}}$, and it is appropriate to think of $\Delta\omega_{\mathrm{NR}}/2\pi$ as arising solely from the CPB's state-dependent polarizability or 'quantum capacitance'[22,23]. Thus, for fixed E_{J}, $|\Delta\omega_{\mathrm{NR}}/2\pi|$ is always maximized at CPB charge degeneracy points, $E_{\mathrm{el}} = 0$, where the magnitude of the state-dependent component of the quantum capacitance is greatest.

We cool the sample to a temperature in the range of $T_{\mathrm{mc}} \approx 100$–140 mK, where the qubit predominantly resides in the ground state (that is, $k_{\mathrm{B}}T_{\mathrm{mc}} \ll \Delta E$, where k_{B} is Boltzmann's constant) and the rate of quasiparticle poisoning in the qubit is minimal[24]. We then measure the nanoresonator frequency response using a combination of capacitive displacement transduction and radio-frequency reflectometry[25] (Fig. 1b and Supplementary Information). Figure 1c shows the frequency response of the nanoresonator amplitude (main panel) and phase (upper inset) at two values of V_{CPB} for fixed Φ and $V_{\mathrm{NR}} = 15$ V (the largest coupling voltage used in the experiment). Consistent with equation (3) and the CPB residing in the ground state, when V_{CPB} is adjusted to a charge degeneracy point, the nanoresonator experiences a decrease in frequency, the magnitude of which is found to be $|\Delta\omega_{\mathrm{NR}}/2\pi| \approx \hbar\lambda^2/\pi E_{\mathrm{J}} = 1{,}600$ Hz. For fixed values of E_{J} and E_{el}, in agreement with equations (1) and (3), $|\Delta\omega_{\mathrm{NR}}/2\pi|$ is found to exhibit a quadratic dependence on V_{NR} (Fig. 1c, lower inset) over the full range of V_{NR} values used in the experiment.

Embedding the nanoresonator in a phase-locked loop, we can track $\Delta\omega_{\mathrm{NR}}/2\pi$ while keeping V_{NR} fixed and adiabatically sweeping V_{CPB} and Φ (Fig. 2a). The overall dependence of $\Delta\omega_{\mathrm{NR}}/2\pi$ on V_{CPB} and Φ is in excellent qualitative agreement with our model (equation (3) and Fig. 2b–d). We find that $\Delta\omega_{\mathrm{NR}}/2\pi$ exhibits the expected period-2e dependence on V_{CPB}, confirmed for four periods (Supplementary Information). We also observe that the periodicity of $\Delta\omega_{\mathrm{NR}}/2\pi$ in Φ is in good agreement with one flux quantum Φ_o (Supplementary Information), as expected from the Φ dependence of E_{J}. At values of Φ for which $E_{\mathrm{J}}/k_{\mathrm{B}} \lesssim T_{\mathrm{mc}}$ (for example trace 1 in Fig. 2c), the CPB excited state becomes thermally populated in the vicinity of the charge degeneracy points. As a result, the modulation depth of $\Delta\omega_{\mathrm{NR}}/2\pi$ is reduced, which can be accounted for by replacing the qubit expectation in equation (3) with the Boltzmann-weighted average, $\langle\hat{\sigma}_z\rangle = -\tanh(\Delta E/2k_{\mathrm{B}}T_{\mathrm{mc}})$.

We can also manipulate the CPB state $\langle\hat{\sigma}_z\rangle$ by irradiating the CPB gate with microwaves that are resonant with the qubit transition, ΔE, and perform spectroscopy by monitoring the mechanical frequency shift, $\Delta\omega_{\mathrm{NR}}/2\pi$. With the microwave frequency, $\omega_\mu/2\pi$, held fixed and the microwave amplitude, V_μ, adjusted such that polarization charge due to the microwave signal (in units of $2e$) satisfies $n_\mu = C_{\mathrm{CPB}}V_\mu/2e \ll 1$, the CPB will oscillate between $|+\rangle$ and $|-\rangle$ with Rabi frequency $\Omega_{\mathrm{d}} \approx 4E_{\mathrm{C}}E_{\mathrm{J}}n_\mu/\hbar\Delta E$ when V_{CPB} and Φ are tuned such that $\Delta E \approx \hbar\omega_\mu$. Because the response time of the nanoresonator, $2\pi/\kappa$, is long in comparison with characteristic timescales of the CPB's dynamics, measurements of $\Delta\omega_{\mathrm{NR}}/2\pi$ will reflect the average qubit occupation, $\langle\hat{\sigma}_z\rangle = \rho_+ - \rho_-$, where ρ_+ and ρ_- are found from the steady-state solution to the Bloch equations[26]

$$\rho_+ = 1 - \rho_- = \frac{1}{2}\frac{\Omega_{\mathrm{d}}^2 T_1 T_2}{1 + \Omega_{\mathrm{d}}^2 T_1 T_2 + (\Delta E/\hbar - \omega_\mu)^2 T_2^2} \qquad (4)$$

and T_1 and T_2 are the qubit relaxation and dephasing times, respectively. For values of n_μ large enough that $\Omega_{\mathrm{d}}^2 T_1 T_2 \gg 1$, the CPB

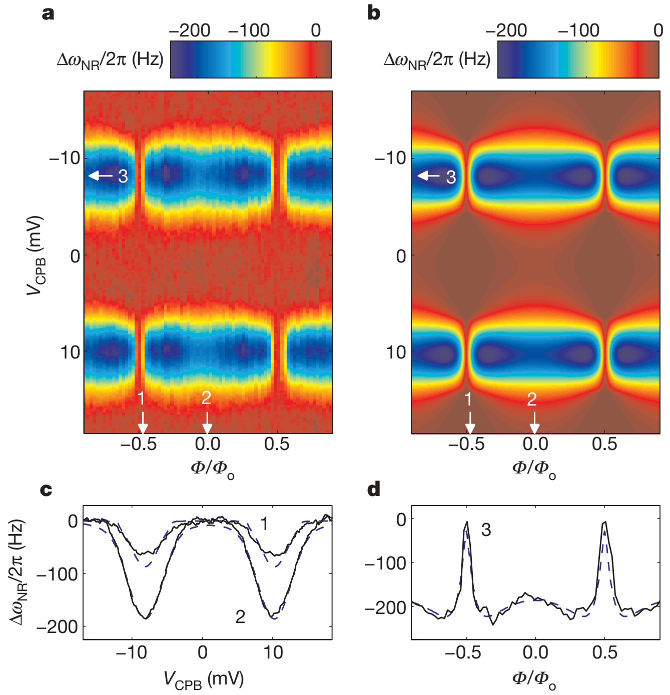

Figure 2 | Nanoresonator frequency shift as function of CPB parameters V_{CPB} and Φ/Φ_o. **a**, Measured $\Delta\omega_{NR}/2\pi$ for $V_{NR} = 7$ V and $T_{mc} \approx 100$ mK. Data has been post-processed to correct for charge drift and background fluctuations in $\omega_{NR}/2\pi$ (Supplementary Information). Normalization of the *x* axis is also discussed in the Supplementary Information. **b**, Numerically calculated $\Delta\omega_{NR}/2\pi$ as a function of V_{CPB} and Φ for $E_C/h = 14.0$ GHz, $E_{J0}/h = 13.2$ GHz and $|\lambda/2\pi| = 1.40$ MHz. The numerical model uses the full CPB Hamiltonian (Supplementary Information) to calculate the two lowest CPB eigenstates, $|+\rangle$ and $|-\rangle$. The CPB population, $\langle\hat{\sigma}_z\rangle$, is then calculated assuming the appropriate Boltzmann weighting. To account for low-frequency charge noise, $\Delta\omega_{NR}/2\pi$ from the model is convolved with a Gaussian of width $\sigma(2e) = 0.10$ in n_{CPB}. **c**, Comparison between data (solid black lines) and model (dashed blue lines) of selected traces of $\Delta\omega_{NR}/2\pi$ versus V_{CPB} for Φ biased near minimum E_J (labelled '1') and maximum E_J (labelled '2') . **d**, Comparison between data (solid black lines) and model (dashed blue lines) of $\Delta\omega_{NR}/2\pi$ versus Φ for V_{CPB} biased on a charge degeneracy (labelled '3').

becomes saturated, that is, $\rho_+ = \rho_- = 1/2$, and $\Delta\omega_{NR}/2\pi \to 0$. Thus, we can perform spectroscopy of the CPB by fixing $\omega_\mu/2\pi$ and n_μ and monitoring the nanomechanical frequency shift $\Delta\omega_{NR}/2\pi$ while adiabatically sweeping V_{CPB} and Φ (Fig. 3a–d). For $\omega_\mu/2\pi = 10.5$–20 GHz, we observe hyperbolae where $\Delta\omega_{NR}/2\pi \to 0$. These trace out constant-energy contours that are in general agreement with the expected n_{CPB}–Φ dependence of the qubit transition, ΔE (Fig. 3e). This allows us to extract the values $E_C/h = 12.7$–13.7 GHz and $E_{J0}/h \approx 13$ GHz (Supplementary Information), which, through equation (3), can be used to estimate the coupling strength, $|\lambda/2\pi| \approx 0.5$–3 MHz over the range $V_{NR} = 2$–15 V. Measurements of the qubit's linewidth, $\gamma/2\pi$, for varying microwave amplitude allow us to determine that $T_2 \geq 2$ ns at charge degeneracy (Supplementary Information).

At large microwave amplitude V_μ ($n_\mu \gtrsim \pi E_J^2/16\hbar\omega_\mu E_C$), we demonstrate that we can utilize the nanomechanical frequency shift, $\Delta\omega_{NR}/2\pi$, as a probe of quantum coherent interference effects in the CPB (Fig. 4). These effects arise as a result of Landau–Zener tunnelling[27] that can occur between $|-\rangle$ and $|+\rangle$ whenever the CPB is swept, by means of V_μ, through the avoided-level crossing at charge degeneracy. If T_2 is greater than the microwave modulation period, $2\pi/\omega_\mu$, then successive Landau–Zener events can interfere, resulting in oscillations in the qubit population, $\langle\hat{\sigma}_z\rangle$, as a function of V_μ and V_{CPB}.

By monitoring $\Delta\omega_{NR}/2\pi$ while sweeping V_{CPB} at fixed values of V_μ, we clearly observe quantum interference (Fig. 4a). At the lowest

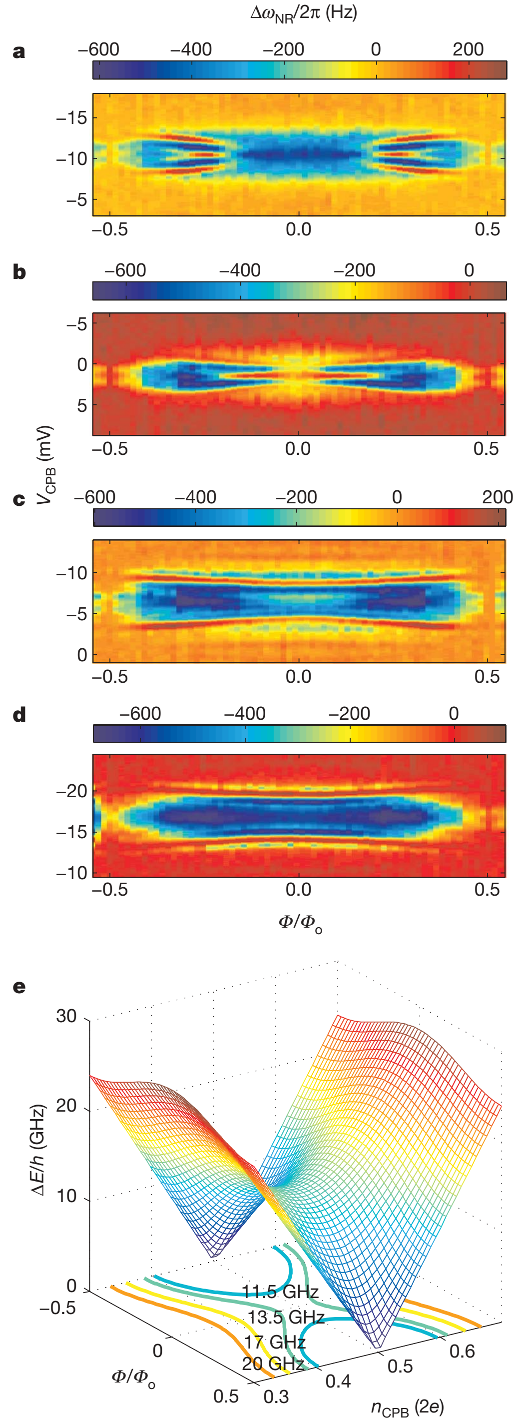

Figure 3 | Spectroscopy of the CPB using the nanomechanical frequency shift as a probe. **a–d**, $\Delta\omega_{NR}/2\pi$ measured as a function of V_{CPB} and Φ while applying microwaves of frequency $\omega_\mu/2\pi = 11.5$ GHz (**a**), 13.5 GHz (**b**), 17 GHz (**c**) and 20 GHz (**d**). Data has been post-processed to correct for charge drift and background fluctuations in $\omega_{NR}/2\pi$ (Supplementary Information). Normalization of the *x* axes is also discussed in the Supplementary Information. Data was taken for $V_{NR} = 10$ V and $T_{mc} \approx 140$ mK. **e**, Surface plot of CPB ground-state/excited-state splitting transition frequency, $\Delta E/h$, as a function of V_{CPB} and Φ, with constant energy contours at the microwave frequencies highlighted.

values of V_μ, Landau–Zener tunnelling is exponentially suppressed[27], and we observe a dependence of $\Delta\omega_{NR}/2\pi$ on V_{CPB} consistent with the CPB residing in $|-\rangle$. As V_μ is increased, we observe that $\Delta\omega_{NR}/2\pi$ oscillates with V_μ and V_{CPB}, even changing sign, and becoming maximally positive at values of V_μ and V_{CPB} for which we expect the occupation of $|+\rangle$ to be a maximum (the intersections of the

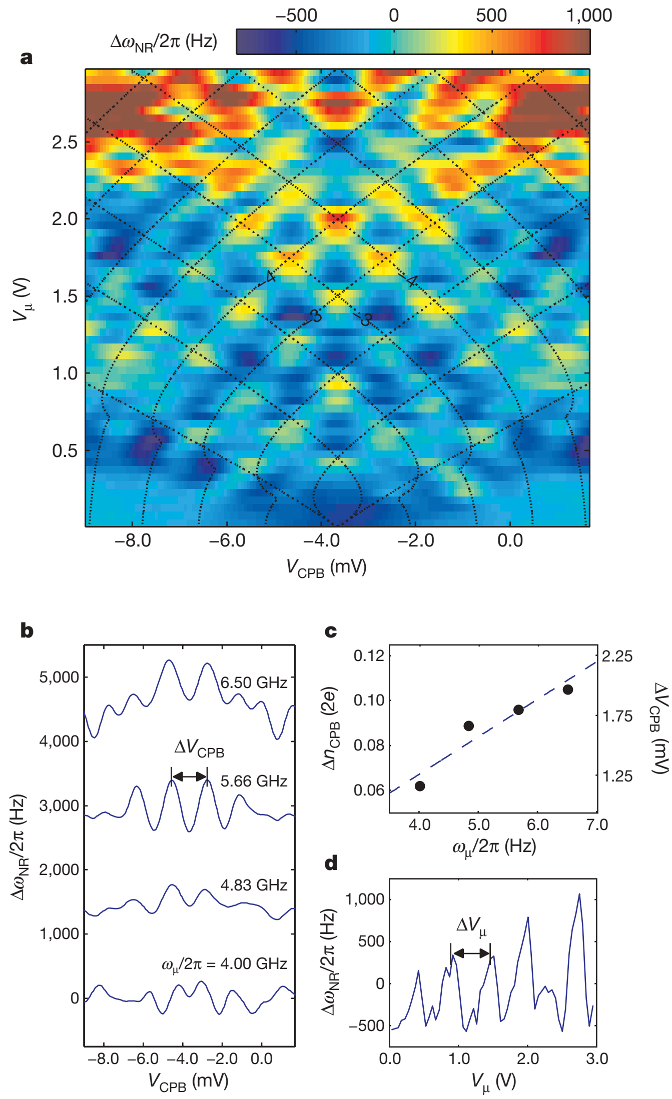

Figure 4 | Landau–Zener interferometry using the nanomechanical frequency shift as a probe. **a**, Interference fringes in $\Delta\omega_{NR}/2\pi$ plotted as a function of microwave amplitude, V_μ, and CPB gate voltage, V_{CPB}, for $\omega_\mu/2\pi = 6.50$ GHz. Data has been post-processed for charge drift (Supplementary Information). The colour scale is saturated at $\Delta\omega_{NR}/2\pi = +1{,}000$ Hz to enhance contrast of fringes at smaller values of V_μ. **b**, Cross-sections for constant values of V_μ, for $\omega_\mu/2\pi = 4.00$–6.50 GHz, chosen to coincide with the intersection of the $m = -3$ and $m = -4$ constant-phase contours, for $2\pi m$ advancement in the phase of the CPB wavefunction (Supplementary Information). The traces at different values of $\omega_\mu/2\pi$ have been offset vertically for clarity, and charge drift between data sets has been subtracted. **c**, Linear fit through the origin of the spacing, Δn_{CPB}, between adjacent interference fringes at the intersection of the $m = -3$ and $m = -4$ constant-phase contours. ΔV_{CPB} is determined from a fit of the interference fringes to a series of Gaussian peaks, and then converted to Δn_{CPB} using the CPB gate capacitance, $C_{CPB} = 17.1$ aF. Error bars are calculated from the Gaussian fit but are smaller than the point size and the scatter in the data, which is probably due to low-frequency charge noise. **d**, Nanomechanical frequency shift versus microwave amplitude for $\omega_\mu/2\pi = 6.50$ GHz at $V_{CPB} = -3.66$ mV, demonstrating the expected periodic modulation of the interference fringes. Data was taken for $V_{NR} = 10$ V and $T_{mc} \approx 110$ mK.

contours in Fig. 4a; Supplementary Information). We observe that the spacing, ΔV_{CPB}, in gate voltage between adjacent interference fringes increases linearly with increasing microwave frequency, $\omega_\mu/2\pi$, as expected[27] (Fig. 4b, c). A linear fit of Δn_{CPB} to $\omega_\mu/2\pi$ (Fig. 4c) yields $E_C/h = 14.9 \pm 0.6$ GHz (s.e.m.) in good agreement with the value extracted from spectroscopy. Figure 4d shows a cross-section of $\Delta\omega_{NR}/2\pi$ as a function of V_μ at charge degeneracy, demonstrating the expected periodic dependence of the interference maxima. The primary maxima in $\Delta\omega_{NR}/2\pi$ occur for values of V_μ that produce a phase shift of $2\pi m$ (where m is an integer) in the CPB's wavefunction over one-half cycle of microwave modulation. The resulting average spacing between peaks, ΔV_μ, found from a fit of the data to a series of Lorentzians, provides an estimated total attenuation of 45 ± 2 dB (s.e.m.) at $\omega_\mu/2\pi = 6.50$ GHz in the CPB gate line, which is in reasonable agreement with measurements of the attenuation made before cool-down with the apparatus at ~300 K (~50–54 dB). It should be possible to extract the qubit dephasing time, T_2, from the width of the interference fringes by using a model that carefully considers the various timescales in the problem (that is, T_1, $2\pi/\omega_\mu$ and $2\pi/\omega_{NR}$)[27].

For both driven and non-driven CPB cases, it is notable how well the simple dispersive model (equation (2)) agrees with our observations. It is not obvious, a priori, that the equations of motion used to model the interaction between an atom and a photon should also apply to the interaction between a suspended nanostructure and a mesoscopic electronic device, in particular because the latter systems each comprise billions of atoms. Despite this agreement, several outstanding issues are noteworthy. First, we observe increased damping of the NEMS upon tuning the CPB to the charge degeneracy point. Although further explorations are necessary to determine the origin of this excess energy loss, the fact that it depends on the CPB gate bias, V_{CPB}, and increases with V_{NR} suggests that it is mediated by the CPB. Second, we observe additional resonant features near charge degeneracy (Fig. 3 and Supplementary Information) whose origins are not yet understood. These robust features do not appear to be sensitive to time or background electric field. Furthermore, they also do not demonstrate a clear dependence on n_μ, suggesting that mechanisms such as multiphoton transitions[19] and Landau-Zener tunnelling[27] may be ruled out.

The dispersive interaction that we have measured, in conjunction with techniques that have been used to manipulate[28] and measure[18,28] superconducting qubits, could soon be used to generate and probe entangled states of nanomechanical systems and qubits. For example, a superposition of nanoresonator coherent states oscillating at distinct frequencies dressed by the state of the CPB (that is, $\omega_{NR,\pm}/2\pi = \omega_{NR}/2\pi \pm \Delta\omega_{NR}/2\pi$) could be generated by dispersively coupling the nanoresonator to a CPB that is initially prepared in a superposition of $|-\rangle$ and $|+\rangle$ (refs 12, 13). Coherence of the nanomechanical system would manifest itself in periodic reductions in and revivals of the coherent oscillations of the qubit as the phases of the two nanoresonator states shift out of alignment and back. This could then be quantified either through careful measurements of the qubit's dephasing spectrum[12,18] or using qubit 'echo' techniques[13,28].

Theoretical investigations of the second approach suggest that entanglement 'recoherences' should be observable in systems similar to ours using a coupling strength of $|\lambda/2\pi| \approx 10$ MHz (ref. 13). This would require a modest improvement to the existing sample, which we anticipate is achievable by engineering a smaller gap electrode; for example, an order-of-magnitude increase in λ is expected using parameters similar to those already demonstrated with single-electron transistors[29]. It will also be necessary to reduce the effects of quasiparticle poisoning and other sources of charge noise to achieve CPB dephasing times $T_2 \gtrsim 100$ ns. This has been accomplished in circuit QED through careful engineering of the CPB's parameters and by using a superconducting cavity for isolation and measurement of the CPB[18,28]. Reducing quasiparticle poisoning will have the additional benefit of enabling operation of the experiment at lower temperatures, where the deleterious effects of the nanoresonator's thermal fluctuations on the visibility of qubit revivals should be much weaker. The calculations in ref. 13 indicate that recoherences should be observable for nanoresonator thermal occupation factors up to ~20, which corresponds to $T_{mc} \lesssim 60$ mK for $\omega_{NR}/2\pi \approx 60$ MHz. This is readily attainable with our dilution refrigerator.

We have demonstrated the read-out of a superconducting qubit using a dispersive interaction with a nanomechanical resonator. This technique joins cantilever-based magnetic resonance force detection[30] as the only demonstrated mechanical probe techniques of individual two-level quantum systems. The realistic prospects of investigating quantum coherence in a nanomechanical resonator establish the nanoresonator-coupled qubit as a valuable new tool with which to explore further the frontiers of quantum mechanics.

Received 24 December 2008; accepted 23 April 2009.

1. Armour, A. D., Blencowe, M. P. & Schwab, K. C. Entanglement and decoherence of a micromechanical resonator via coupling to a Cooper-pair box. *Phys. Rev. Lett.* **88,** 148301 (2002).
2. Irish, E. K. & Schwab, K. C. Quantum measurement of a coupled nanomechanical resonator-Cooper-pair box system. *Phys. Rev. B* **68,** 155311 (2003).
3. Martin, I., Shnirman, A., Tian, L. & Zoller, P. Ground state cooling of mechanical resonators. *Phys. Rev. B* **69,** 125339 (2004).
4. Cleland, A. N. & Geller, M. R. Superconducting qubit storage and entanglement with nanomechanical resonators. *Phys. Rev. Lett.* **93,** 070501 (2004).
5. Tian, L. Entanglement from a nanomechanical resonator weakly coupled to a single Cooper-pair box. *Phys. Rev. B* **72,** 195411 (2005).
6. Buks, E. & Blencowe, M. P. Decoherence and recoherence in a vibrating rf SQUID. *Phys. Rev. B* **74,** 174504 (2006).
7. Wei, L. F. Liu, Y.-x., Sun, C. P. & Nori, F. Probing tiny motions of nanomechanical resonators: classical or quantum mechanical? *Phys. Rev. Lett.* **97,** 237201 (2006).
8. Jacobs, K., Lougovski, P. & Blencowe, M. P. Continuous measurement of the energy eigenstates of a nanomechanical resonator without a non-demolition probe. *Phys. Rev. Lett.* **98,** 147201 (2007).
9. Clerk, A. A. & Utami, D. W. Using a qubit to measure photon-number statistics of a driven thermal oscillator. *Phys. Rev. A* **75,** 042302 (2007).
10. Hauss, J. *et al.* Single-qubit lasing and cooling at the Rabi frequency. *Phys. Rev. Lett.* **100,** 037003 (2008).
11. Jacobs, K., Jordan, A. N. & Irish, E. K. Energy measurements and preparation of canonical phase states of a nano-mechanical resonator. *Europhys. Lett.* **82,** 18003 (2008).
12. Utami, D. W. & Clerk, A. A. Entanglement dynamics in a dispersively coupled qubit oscillator system. *Phys. Rev. A* **78,** 042323 (2008).
13. Armour, A. D. & Blencowe, M. P. Probing the quantum coherence of a nanomechanical resonator using a superconducting qubit: I. Echo scheme. *N. J. Phys.* **10,** 095004 (2008).
14. Haroche, S. & Raimond, J. M. *Exploring the Quantum: Atoms, Cavities, and Photons* (Oxford Univ. Press, 2006).
15. Heinzen, D. J. & Feld, M. S. Vacuum radiative level shift and spontaneous-emission linewidth of an atom in an optical resonator. *Phys. Rev. Lett.* **59,** 2623–2626 (1987).
16. Guerlin, C. *et al.* Progressive field-state collapse and quantum non-demolition photon counting. *Nature* **448,** 889–893 (2007).
17. Brune, M. *et al.* Observing the progressive decoherence of the "meter" in a quantum measurement. *Phys. Rev. Lett.* **77,** 4887–4890 (1996).
18. Schuster, D. I. *et al.* Resolving photon number states in a superconducting circuit. *Nature* **445,** 515–518 (2007).
19. Wilson, C. M. *et al.* Coherence times of dressed states of a superconducting qubit under extreme driving. *Phys. Rev. Lett.* **98,** 257003 (2007).
20. Nakamura, Y., Pashkin, A. & Tsai, J. S. Coherent control of macroscopic quantum states in a single-Cooper-pair box. *Nature* **398,** 786–788 (1999).
21. Makhlin, Y., Schon, G. & Shnirman, A. Quantum-state engineering with Josephson junction devices. *Rev. Mod. Phys.* **73,** 357–400 (2001).
22. Sillanpaa, M. A. *et al.* Direct observation of Josephson capacitance. *Phys. Rev. Lett.* **95,** 206806 (2005).
23. Duty, T. *et al.* Observation of quantum capacitance in the Cooper-pair transistor. *Phys. Rev. Lett.* **95,** 206807 (2005).
24. Palmer, B. S. *et al.* Steady-state thermodynamics of non-equilibrium quasiparticles in a Cooper-pair box. *Phys. Rev. B* **76,** 054501 (2007).
25. Truitt, P. A. *et al.* Efficient and sensitive capacitive readout of nanomechanical resonator arrays. *Nano Lett.* **7,** 120–126 (2007).
26. Schuster, D. I. *et al.* ac Stark shift and dephasing of a superconducting qubit strongly coupled to a cavity field. *Phys. Rev. Lett.* **94,** 123602 (2005).
27. Sillanpaa, M. *et al.* Continuous-time monitoring of Landau-Zener interference in a Cooper-pair box. *Phys. Rev. Lett.* **96,** 187002 (2006).
28. Leek, P. J. *et al.* Observation of Berry's phase in a solid-state qubit. *Science* **318,** 1889–1892 (2007).
29. Naik, A. *et al.* Cooling a nanomechanical resonator with quantum back-action. *Nature* **443,** 193–196 (2006).
30. Rugar, D., Budakian, R., Mamin, H. J. & Chui, B. W. Single spin detection by magnetic resonance force microscopy. *Nature* **430,** 329–332 (2004).

Supplementary Information is linked to the online version of the paper at www.nature.com/nature.

Acknowledgements The authors would like to thank T. Duty, C. Wilson, G. Milburn, A. Doherty, E. Babourina-Brooks, A. Armour, A. Clerk and I. Bargatin for discussions; S. Stryker and A. Sears for assistance in constructing the measurement apparatus; and R. E. Muller for electron beam lithography. K.C.S. acknowledges support from the US National Science Foundation (DMR-0804567) and the Foundational Questions Institute (RFP2-08-27). M.D.L. acknowledges support from the Center for the Physics of Information, California Institute of Technology. Part of the research described in this publication was carried out at the Jet Propulsion Laboratory, California Institute of Technology, under a contract with the US National Aeronautics and Space Administration.

Author Information Reprints and permissions information is available at www.nature.com/reprints. Correspondence and requests for materials should be addressed to M.L.R. (roukes@caltech.edu).